GEOPHYSICAL RESEARCH LETTERS, VOL. 16, NO. 5, PAGES 413-416, MAY 1989

# TELESEISMIC INVESTIGATION OF THE JANUARY 22, 1988 TENNANT CREEK, AUSTRALIA, EARTHQUAKES

Robert McCaffrey

Department of Geology, Rensselaer Polytechnic Institute, Troy

*Abstract.* The three January 22, 1988, earthquakes are the largest to occur within the Australian continent in 20 years and produced two colinear but discontinuous WNW trending scarps enclosing a shorter ENE trending scarp. Teleseismic long period P and SH and short period P waves are used to constrain the locations and source parameters for the three events. The third earthquake has a seismic moment ($10^{19}$Nm) equal to that of the 1968 Meckering event and most likely ruptured the southern of the WNW trending faults. Relative relocations suggest that the two smaller earthquakes initiated north or NW of the third event. Centroid depths are less than 6 km, but most likely 3 to 4 km, and source durations are 4 to 6s so it is probable that each event broke the surface. All three earthquakes have predominantly thrust mechanisms and nodal planes that strike west to WNW, consistent with faults dipping southward at 30° to 40°. Only the first has a nodal plane that could support a north dip for the ENE trending fault, as proposed by other researchers on the basis of ground deformation and preliminary aftershock locations. However, source directivity evident in the short period P waves and relocations are interpreted better if this event, like the others, ruptured a SW dipping fault plane. The ENE trending scarp is interpreted to be a tear fault in the hanging wall that may have acted as a barrier to slip on a single continuous SW dipping fault, resulting in this unusual, at least for Australia, sequence of three large similar earthquakes.

## Introduction

The Australian continent is not known for its great seismic activity yet it occasionally produces large earthquakes with impressive ground breakage. The largest well-studied event was the Meckering thrust earthquake of 1968 which produced a 30 km long fault scarp with up to 2m of slip [Gordon and Lewis 1980]. These earthquakes are also unusual in that they have centroid depths of only a few kilometers, which indicates that faulting is contained in the upper part of the crust [Frederich et al. 1988].

On January 22, 1988, three large earthquakes occurred within a period of 12 hours in north central Australia. The first two events, here called TC1 and TC2, were of $m_b$=6.1 ($M_s$=6.3) and the third, TC3, was $m_b$=6.5 ($M_s$=6.7). These earthquakes comprise three of the four largest in Australia during the last 25 years. The occurrence of three large closely related events is atypical of Australian earthquakes; to now they have occurred as single large events accompanied by many others of significantly lower magnitudes.

The January 1988 earthquakes created two major fault scarps [Bowman 1988a]; a southern one called the Lake Surprise (LS) scarp displaying a boomerang shape in map view and the Kunayungku (K) scarp in the north (Figure 1). On the WNW trending scarps, the south side was lifted as much as 2m relative to the north side and a trench across the LS scarp revealed a thrust plane dipping 20 to 30°S. Gas company employees found no scarp when surveying the pipeline (Figure 1) between the first and third events [Bowman 1988b]. Bowman et al. [1988] describe aftershock zones dipping to the SW at 40 to 50° from the WNW trending surface breaks. The ENE trending West Lake Surprise (WLS) scarp displayed some left lateral strike slip motion but was also predominantly dip slip. Slip on the WLS fault from field observations, while more variable, was inferred to be north-side-up, opposite to that observed on the WNW trending scarps [Bowman 1988a]. Bowman et al. [1988] interpret the preliminary locations of aftershocks as defining a NW dip for the WLS fault and infer that it is a thrust fault.



Paper number 89GL00567.
0094-8276/89/89GL-00567$03.00

## Waveform Data and Analysis

Seismograms for the three earthquakes were obtained by writing to World Wide Standardized Seismograph Network (WWSSN) stations. P wave first motions and arrival times were read from many short and long period seismograms and others were supplied by network operators in Indonesia and Papua New Guinea.

For all three events the short period signal is contained in the first five to ten seconds indicating that the sources are both shallow and short in duration (Figure 2). The SH waves are on the average twice the amplitude of the P waves (Figure 3; note the different amplitude scales for P and SH), typical of strike slip and very shallow dip slip earthquakes. First motions indicate thrust mechanisms (Figure 3) but regional seismograms reveal some variations in them (Figure 2). The long period vertical seismograms for all three events from ADE and MUN are similar for most of the signal but in the first half cycle differences in the amplitude of the direct P wave are clear. PMG seismograms display similar variations.

Short period arrival times are used to identify the start of the P wave on the long period seismograms because the proper alignment is necessary to obtain the correct mechanism and depth. For TC1 and TC3 the long period and short period P waves start simultaneously but for TC2 the long period first motions appear to be delayed by several seconds with respect to those of the short period (Figure 2). While this apparent delay of the long period can be caused by a nodal arrival, the observation that the long period P at WEL is also delayed with respect to the short period even though WEL is far from the node (Figure 3) shows that the source time function for event TC2 contributes to the emergent nature of the seismograms.

The faulting parameters for the three earthquakes (Table 1) were constrained by least-squares inversion of the waveforms. Long peri-

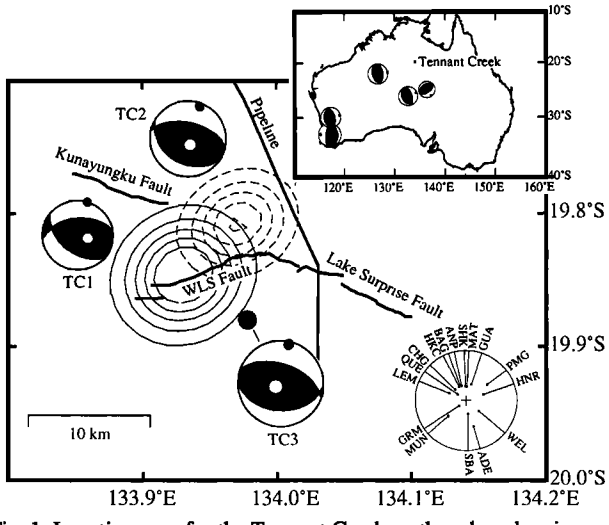


Fig. 1. Location map for the Tennant Creek earthquakes showing the traces of the fault scarps (WLS=West Lake Surprise) and the best fitting fault plane solutions. The radii of the focal spheres are scaled to the log of the seismic moment. Also shown are the contours of the probability density function for the locations of TC1 (solid contours) and TC2 (dashed contours) relative to TC3 (preferred location shown by a dot). The contour interval is 20%. At the lower right, locations of seismograph stations are shown on the focal sphere. (Inset) The location of Tennant Creek and fault plane solutions of the largest earthquakes in the Australian continent in the past 25 years [Frederich et al. 1988].

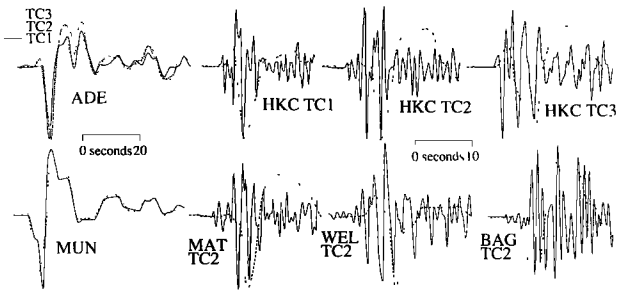


Fig. 2. Sample seismograms from the Tennant Creek earthquakes. For the 6 seismograms on the right the short period (solid lines) and the long period (dashed) are plotted at the same time scale and superimposed. In this figure only, seismograms have been normalized by their maximum amplitudes.

od P and SH (Figure 3) and short period P (Figure 4) waveforms were inverted simultaneously for a point-source double couple mechanism (strike, dip, and rake of the fault plane), the centroid depth, and the amplitudes of overlapping triangles representing the source time function [Nabelek 1984; McCaffrey and Abers 1988]. This method estimates the centroid double couple, which can be thought of as the weighted average of a time varying mechanism, where the weighting factor is the seismic moment. If the fault orientation changed during rupture, the centroid mechanism will differ from that at the initiation of rupture and some first motions may be violated.

The best fitting solutions are largely thrust and, with the exception of TC1, have only a small component of strike slip motion. Despite the variation in mechanisms, the P axes inferred from them are remarkably similar for all three events; their azimuths range only from 16° to 20° (Table 1).

The waveforms constrain centroid depths to be less than 6 km, with the best matches at 3 to 4 km (Figure 3; Table 1). Attempts to place the sources deeper, for example at 9 km, near the bottom of the aftershock zone reported by Bowman et al. [1988], resulted in the solutions becoming strike slip in order to match the high amplitudes of the SH waves relative to the P waves, but the overall fit was degraded (Figure 3).

Unlike those from TC2 and TC3, the short period seismograms for TC1 are matched poorly with a point source (Figure 4, top). The match to the TC2 and TC3 short period seismograms rules out structure as the cause of the complexity in the TC1 seismograms. The compactness and high amplitudes of the HKC and SHK seismograms relative to the point source seismograms suggest that the directivity of the source for TC1 was toward these stations. A line source propagating horizontally toward the WNW produces a better fit (Figure 4; case II) than one propagating westward (case I) but greater agreement occurs when the source propagates toward the NW. A line source propagating updip along the SW dipping nodal plane (case IV) matches the short period seismograms better than

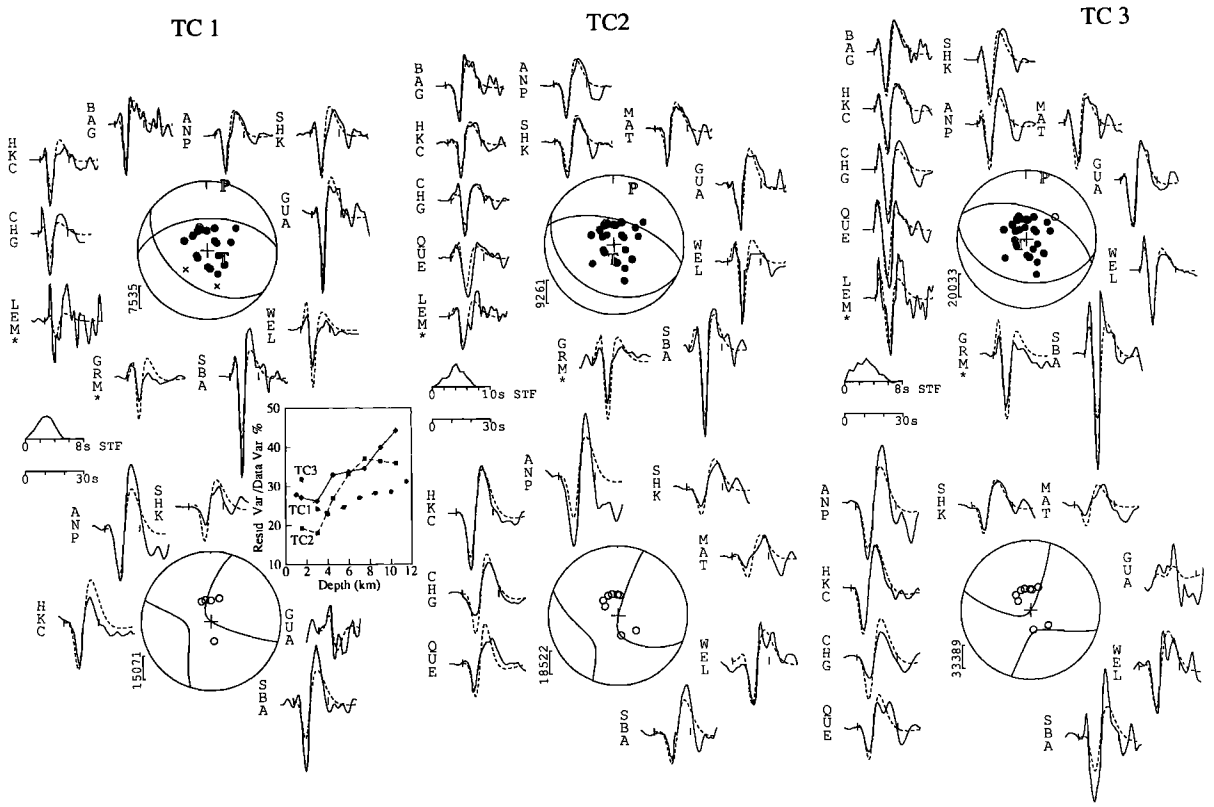


Fig. 3. Fault plane solutions for the three Tennant Creek earthquakes determined by simultaneous inversion of long and short period seismograms. At the top are the long period P waveforms and at the bottom are the SH waveforms. Short period seismograms for these mechanisms are shown in Figure 4. In the top focal sphere, dots represent compressional P wave first motions, circles are dilatations, and x's are nodal arrivals. Solid lines are observed seismograms and dashed lines are calculated. The amplitudes of the WWSSN seismograms are corrected for instrument magnification (x3000), geometrical spreading at a delta of 40°, and attenuation, but are not otherwise normalized (amplitude scales in microns are beside each focal sphere). Resulting source time functions are shown on the axes labeled STF and the other time axis is for the seismograms. Assumed values of t* (travel time/average Q) are 1.0s for P and 4.0s for SH. Stations LEM and GRM are outside the acceptable distance range (30° to 90°) for this technique and are not used. Ticks enclose the portions of the seismograms used in the inversion. Source and receiver structures are halfspaces with $v_p$=6.00 km/s, $v_s$=3.43 km/s, and density of 2.70 g/cm$^3$. The inset plot shows the variance of the residual seismogram amplitudes divided by the variance of the data for a range of depths using point sources. At each depth the waveforms were realigned to maximize fit while keeping the starting time within 1s of the arrival times on short period seismograms. The inversion was then run while all parameters except depth were allowed to change.

TABLE 1. Tennant Creek earthquake double couple point source parameters from waveform analysis

| | Origin Time | Duration, s | Depth, km | Moment, $10^{18}$Nm | Fault Plane Strike | Dip | Rake | Auxiliary Plane Strike | Dip | Rake | P axis Az | Pl | T axis Az | Pl |
|---|---|---|---|---|---|---|---|---|---|---|---|---|---|---|
| TC1 | 0:35:57 | 4.2(0.5) | 2.7(2.6) | 3.66(0.26) | 128(7) | 45(6) | 120(9) | 268(11) | 52(5) | 63(11) | 17 | 3 | 116 | 69 |
| TC2 | 3:57:25 | 5.9(0.5) | 3.0(1.3) | 5.77(0.34) | 117(6) | 30(3) | 100(6) | 286( 6) | 61(3) | 84( 6) | 20 | 15 | 182 | 74 |
| TC3 | 12: 4:58 | 5.4(0.4) | 4.2(1.9) | 9.77(0.61) | 102(8) | 38(2) | 82(7) | 292( 5) | 53(2) | 96( 6) | 18 | 8 | 230 | 81 |

Strike, dip, rake, azimuth (Az), plunge (Pl) angles are given in degrees. Estimated uncertainties are given in parentheses (likely uncertainties are 2 standard deviations for duration and moment, 10 standard deviations for depth, and 5 standard deviations for strike, dip, and rake [Nabelek 1984]).

one moving downdip along the north dipping plane (case III). This preliminary examination suggests that the fault plane for TC1 dips to the SW.

The strikes of both nodal planes for both TC2 and TC3 parallel the trend of the K and LS scarps (110°; Bowman 1988a) within the uncertainties. The south dipping planes are certainly the fault planes. The best overall fit to the waveforms is found for TC2 but its centroid mechanism violates the first motion polarities at BAG and PMG (Figure 3). The short period first motions at HKC and BAG are of opposite polarity (Figure 2) but an inversion performed while the dip of the north dipping plane was forced to fit these first motions (i.e., dip=64°) could not produce an acceptable match to the observed long period seismograms, particularly those P waves to the NW (this trial results in a poorer match to CHG and QUE than that shown in Figure 5). Since the waveform data are sensitive to the episode of faulting in which most of the seismic moment was generated, the inconsistent first motions suggest that the mechanism changed after the onset of faulting. The inclusion of line sources for events TC2 and TC3 did not improve the fits to the waveforms over the point source models.

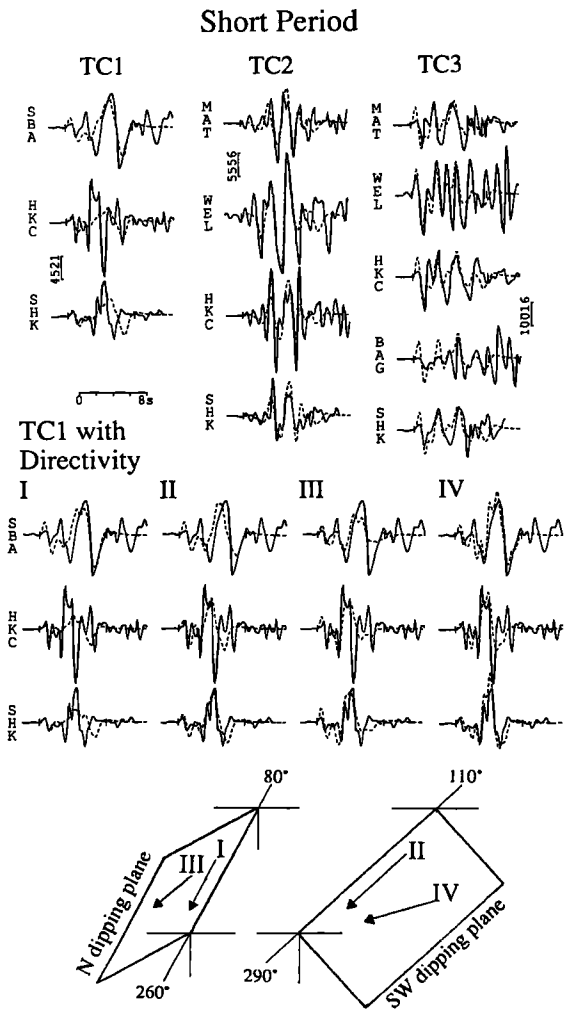


Fig. 4. (top) Observed and calculated short period seismograms for point source solutions shown in Figure 3. Amplitude scales (in microns) correspond to a WWSSN short period instrument at a distance of 40° with a magnification of 25,000. Attenuation was calculated with a t* of 0.7s. (bottom) Short period seismograms for event TC1 using propagating line sources (rupture velocity=2.5 km/s) as shown in the sketch at the bottom: (I) horizontal rupture toward azimuth of 260°; (II) horizontal rupture toward azimuth of 290°; (III) rupture toward azimuth of 330° and down the dip of the north dipping plane; and (IV) rupture toward azimuth of 330° and up the dip of the SW dipping plane. For each trial the inversion was done using all seismograms.

## Relocation

Arrival times are used to calculate probability density functions [Tarantola and Valette 1982] for the relative locations of the three earthquakes using a master event technique. The *a posteriori* probability density function P for the location of the earthquake (with the origin time term removed and assuming gaussian data) is given by

$$P(X,Y,Z)=K\, p(X,Y,Z)\, \exp\{-1/2\, \mathbf{R}^T(C_t+C_m)^{-1}\mathbf{R}\} \qquad (1)$$

where K is the sum of the weights, p is an *a priori* probability density function, **R** is the vector of arrival time residuals with its mean removed, and $C_t$ and $C_m$ are the covariance matrices for the observations and the model, respectively. The errors in the observations $e_t$ and in the model $e_m$ are assumed to be uncorrelated so that $C_t=e_t^2\mathbf{I}$ and $C_m=e_m^2\mathbf{I}$ where **I** is the identity matrix. In our case, the source depth $z_e$ is known independently and the *a priori* density function is $p(X,Y,Z)=1$ for $Z=z_e$, and $p=0$ for other depths.

The data errors $e_t$ are assumed to be 0.5s for arrivals picked by the author from short period records, 1.5s for arrivals from long period seismograms (by cross-correlation with synthetic seismograms), and 2.0s for arrival times picked by others. Because the master event technique uses the difference between two arrival times, these errors are double the normal estimate. The master event approach also eliminates the effects of ray path differences outside the source region, so the model error $e_m$ is that within the source region only, taken to be 0.1s.

The master event TC3 is shown near the LS fault but at a distance to the south consistent with its centroid depth and dip angle (Figure 1). This position is arbitrary but is within the 90% confidence limit for its location determined from arrival times at the Warramunga array, 30 km to the east [Bowman 1988b]. The values of P(X,Y) for the locations of events TC1 and TC2 relative to TC3 were calculated every 0.01° of latitude and longitude and contoured (Figure 1). The contours are circular indicating that the weighted observations are evenly distributed. Using TC2 as the master resulted in similar relative locations of the 3 events but a closer grouping. Because this is a relative location the position of the group of earthquakes with respect to ground features is arbitrary.

The relocated epicenters correspond to the nucleation points for the earthquakes since they are based largely on short period arrival times. Both TC1 and TC2 appear to have nucleated to the north or NW of TC3, which probably ruptured the Lake Surprise (LS) fault. Unless TC3 occurred at the far eastern end of the LS fault, which is unlikely since TC3 seismograms show no finite fault effects, then

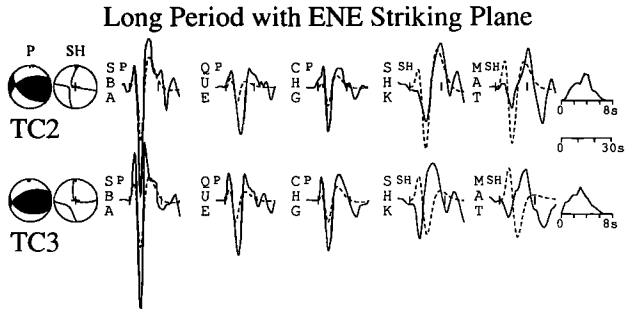


Fig. 5. Seismograms for events TC2 and TC3 showing the misfit when they have an ENE striking, NNW dipping nodal plane corresponding to the WLS fault. For this test the orientation of one nodal plane was constrained (strike=250°, dip=55°NW) and the best fitting values for the remaining parameters (rake angle, depth, and source time function) were determined by inversion of all seismograms.

TC1 and TC2 both started near the western end of the LS fault, as shown in Figure 1.

## Discussion and Conclusions

Given the three apparently distinct segments of ground rupture and the three large earthquakes, one is first tempted to make a one-to-one correspondence. TC1 is the only one of the three events that displays a nodal plane consistent with a north dip on the WLS fault (Figures 1 and 5). The plane striking 268±7° and dipping 52±5°N agrees with the azimuth of the ground break (260°) and aftershocks that apparently define a zone dipping 55°N. The other nodal plane (strike=128±7°, dip=45±6°S) is consistent with the trends of both the K and LS faults (110°) and the dip of the fault planes (50°S and 40°S, respectively) inferred from aftershocks. Evidence against TC1 rupturing the north dipping plane on the WLS fault is the combination of the directivity in the short period P waves, showing a northwestward propagating rupture, and the relocations (Figure 1 and Bowman [1988b]) that place TC1 west of the other events. If TC1 initiated in the west and ruptured westward then this event, if any, occurred on the K fault. The source duration for TC1 (4s for both the point and line sources) corresponds to a fault length of about 10 km, assuming a unilateral rupture with a velocity of 2.5 km/s, which is the distance from the inferred nucleation point for TC1 to the western end of the K scarp (Figure 1). I suggest that TC1 has more of a thrust mechanism than the best-fit solution displays (the available waveforms for TC1 cannot rule out a pure thrust mechanism) and occurred on the K fault.

For TC2, the source time function, which represents the temporal variation of the seismic moment produced by the faulting, is small for 3s, then roughly doubles for another 3s (Figure 3) indicating a sudden doubling of either the fault slip or fault area (the seismic moment is proportional to the product of the average slip and the fault area). TC2 apparently initiated beneath the unbroken region between the LS and K scarps (Figure 1) and ruptured symmetrically. I suggest that the initial 3s of the slip for TC2 was in the region of no ground breakage and that the sudden increase in moment was caused by an increase in the slip that allowed the fault to break the surface at the K or LS scarp or both.

The waveform solution for TC3 agrees closely with the field observations and aftershocks for the eastern LS fault. First, the observed trend of the fault (110°) is similar to the strike of the south dipping plane (102±8°). Second, the dip of the fault inferred from the aftershocks is 40°S while waveforms give a dip of 38±2°S. Third, Bowman [1988a] reports 25-30 cm of left lateral displacement on the LS fault; this is roughly 15-20% of the dip slip component and predicts a rake angle of approximately 80°, in agreement with that found here for TC3 (82±7°). Finally, the centroid depth (4.2±1.9 km) is roughly half the maximum depth of the aftershocks (9 km) reported by Bowman et al. [1988]. The estimated seismic moment for TC3 ($10^{19}$Nm) is comparable to that of the 1968 Meckering earthquake ($M_o$=1.04±0.05x$10^{19}$Nm [Frederich et al. 1988]). This moment predicts an average slip of 1.8m on the LS fault (using a fault length of 12 km and downdip width of 9km/sin(38°)=15 km) which is similar to that observed at the surface.

The apparent anomaly in the Tennant Creek earthquake sequence is the WLS scarp. Evidently it displays north-side-up displacement and has been interpreted as the surface expression of a north dipping thrust fault on the basis of aftershock locations [Bowman et al. 1988]. If so it requires an extremely complex geometry since the K and LS faults dip to the south. As explained above, it is unlikely that any of the three largest January 22 events occurred on such a north dipping thrust fault. At this time, I am disinclined to reject the teleseismic constraints on the basis of unpublished aftershock locations, which are often difficult to interpret, and may not reveal faults that were active during the main faulting episode.

Alternatively, the WLS scarp may represent coseismic or postseismic failure of the hanging wall. Extensive normal faults with throws of several meters were observed in the hanging wall of the 1980 El Asnam earthquake, particularly in the north where only normal faulting was seen at the surface yet geodetic and seismologic data demonstrated that thrust faulting was the dominant mode of deformation [e.g., Nabelek 1985]. If dip slip faulting at the WLS fault was contained within the hanging wall, its seismic moment would be at most 1.3x$10^{18}$ Nm for an average 1m of slip; an earthquake of this size is below the noise level of TC2 and TC3. Recall that short period first motions at stations to the NW for TC2 are consistent with a nodal plane dipping steeply to the NW and not with the centroid solution; perhaps the WLS fault ruptured at the beginning of TC2 but its signal was obscured by a much larger event that followed quickly on a SW dipping fault.

The WLS fault coincides with a quartz ridge; these are known to mark faults in the Proterozoic rocks of NE Australia [Bowman 1988b]. I suggest that the the Kunayungku and Lake Surprise scarps represent the same SW dipping fault in the crust and that all three of the large earthquakes occurred on this fault. The West Lake Surprise fault, a pre-existing weak zone in the hanging wall, created a discontinuity in stress on the fault surface at its intersection with the fault plane. This discontinuity inhibited slip from continuing from the Kunayungku section to the Lake Surprise section, causing multiple events rather than a single large earthquake, which to now has typified large Australian events.

*Acknowledgements.* I thank the many operators of WWSSN stations who sent seismograms, J. Frederich and S. Roecker for assistance, and J.R. Bowman for comments.

## References

Bowman, J.R., The January 22, 1988 Tennant Creek earthquakes: three Ms 6.3-6.7 earthquakes in the Proterozoic shield, *Geol. Soc. Aust. Newsletter, 7*, 3-6, 1988a.

Bowman, J.R., Constraints on the locations of large intraplate earthquakes in the Northern Territory, Australia from observations at the Warramunga seismic array, *Geophys. Res. Lett., 15*, 1475-1478, 1988b.

Bowman, J.R., G. Gibson and T. Jones, Faulting process of the January 22, 1988 Tennant Creek, Northern Territory, Australia earthquakes (abstract), *Eos Trans. AGU, 69*, 1301, 1988.

Fredrich, J., R. McCaffrey and D. Denham, Source parameters of seven large Australian earthquakes determined by body waveform inversion, *Geophys. J., 95*, 1-13, 1988.

Gordon, F., and J. Lewis, The Meckering and Calingiri earthquakes of October 1968 and March 1970, *Bull. Geol. Surv. West Aust. 126*, 1980.

McCaffrey, R., and G. Abers, SYN3: A microcomputer program for inversion of teleseismic body waveforms, *Rep. AFGL-TR-88-0099*, 15 pp., Air Force Geophys. Lab., Bedford, Mass., 1988.

Nabelek, J., Determination of earthquake source parameters from inversion of body waves, Ph.D. thesis, 361 pp., Mass. Inst. of Tech., 1984.

Nabelek, J., Geometry and mechanism of faulting of the 1980 El Asnam, Algeria, earthquake from inversion of teleseismic body waves and comparison with field observations, *J. Geophys. Res., 90*, 12,713-12,728, 1985.

Tarantola, A., and B. Valette, Inverse problems = quest for information, *J. Geophys., 50*, 159-170, 1982.

R. McCaffrey, Department of Geology, Rensselaer Polytechnic Institute, Troy, NY 12180.

(Received January 9, 1989;
Revised March 14, 1989;
Accepted March 17, 1989.)